Supplementary Materials

Figures

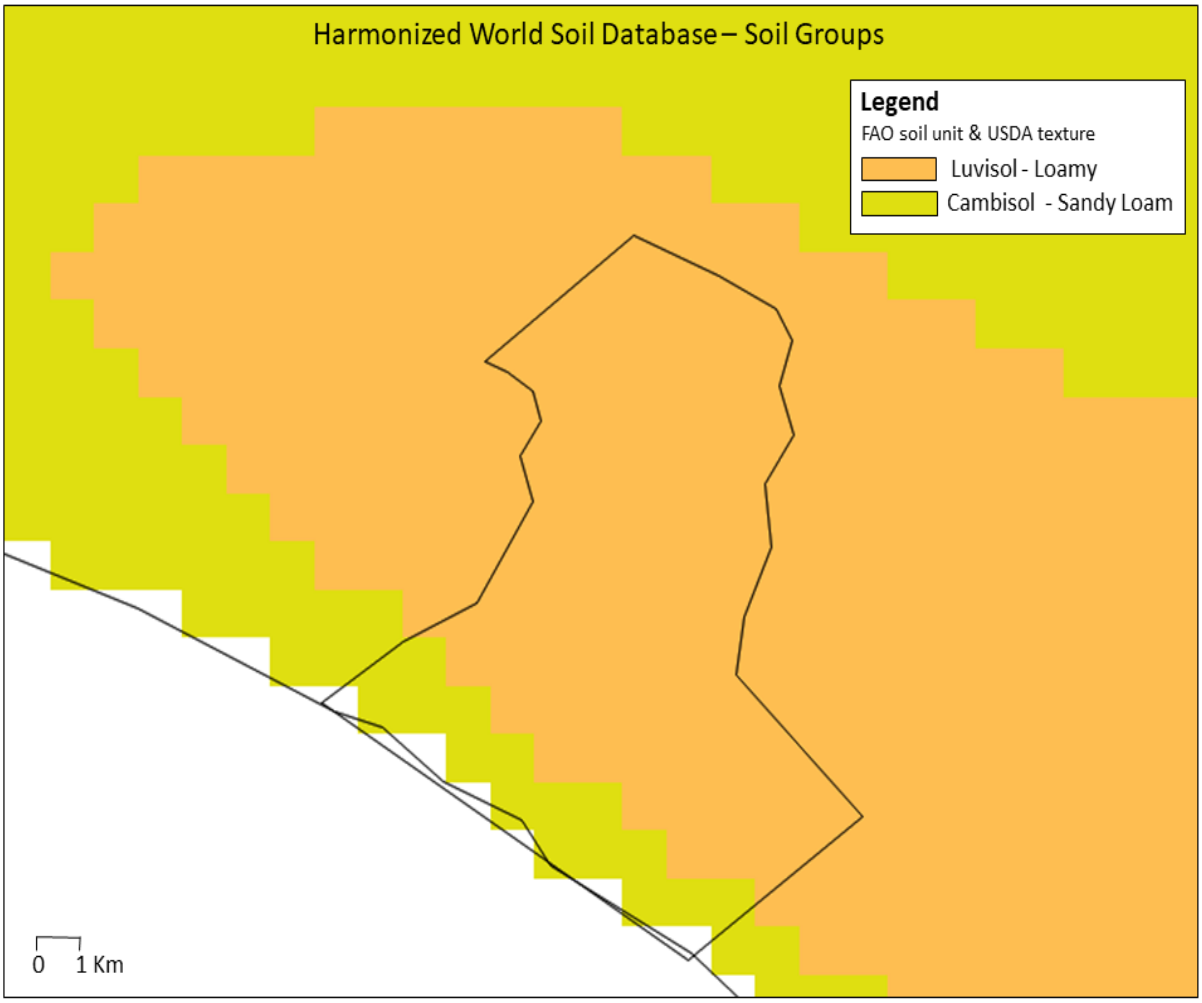

Figure S1. Soil classification for the Castelporziano natural reserve derived from the Harmonized World Soil Database viewer (HWSD v.1.2) is reported. The dominant soil units are Eutric Cambisol (FAO 90) in the coastal area (yellow pixels), characterized by a sandy loam texture (USDA texture classification) with a 77,14, 9 % of sand, silt and clay fraction composition in the first 30 cm (topsoil), respectively. The dominant inland (orange pixels) soil unit is Chromic Luvisol (FAO 90), characterized by a Loamy texture (USDA texture classification) with a 47, 29, 24 % of sand, silt and clay fraction composition in the first 30 cm (topsoil), respectively.

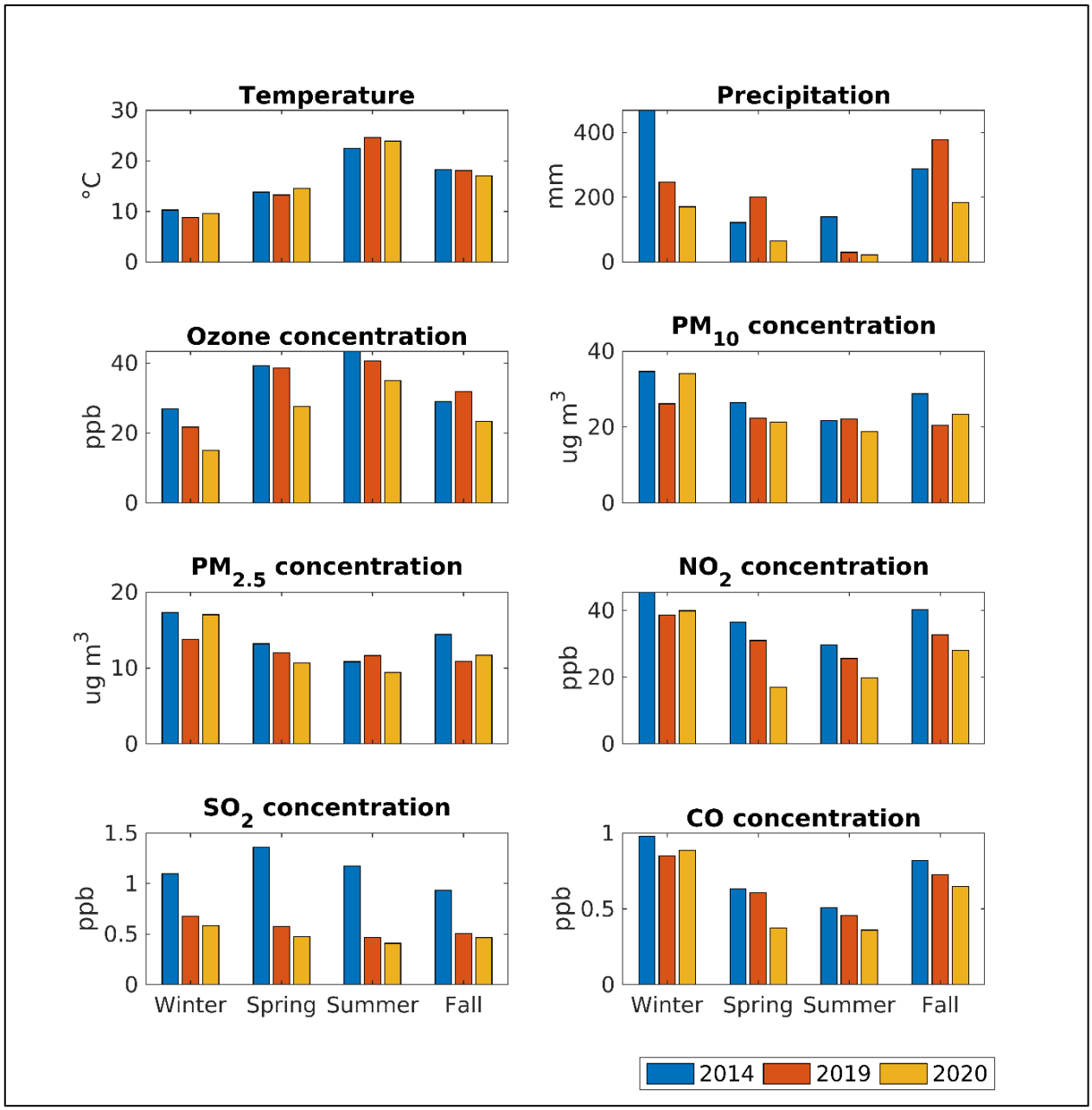

Figure S2. Meteorological inter-comparison between the three years of study seasonal values of mean temperatures, and cumulated precipitation (top left and top right, respectively) are shown together with average concentrations of PM, NO2, SO2 and CO.

Figure S3. Spatial association of meteorological stations to homogeneous portions of the natural reserve. Yellow dots indicate the position of each one of the meteorological stations. Climatic conditions of the portions of the Estate (red shapes) were associated to each meteorological station.

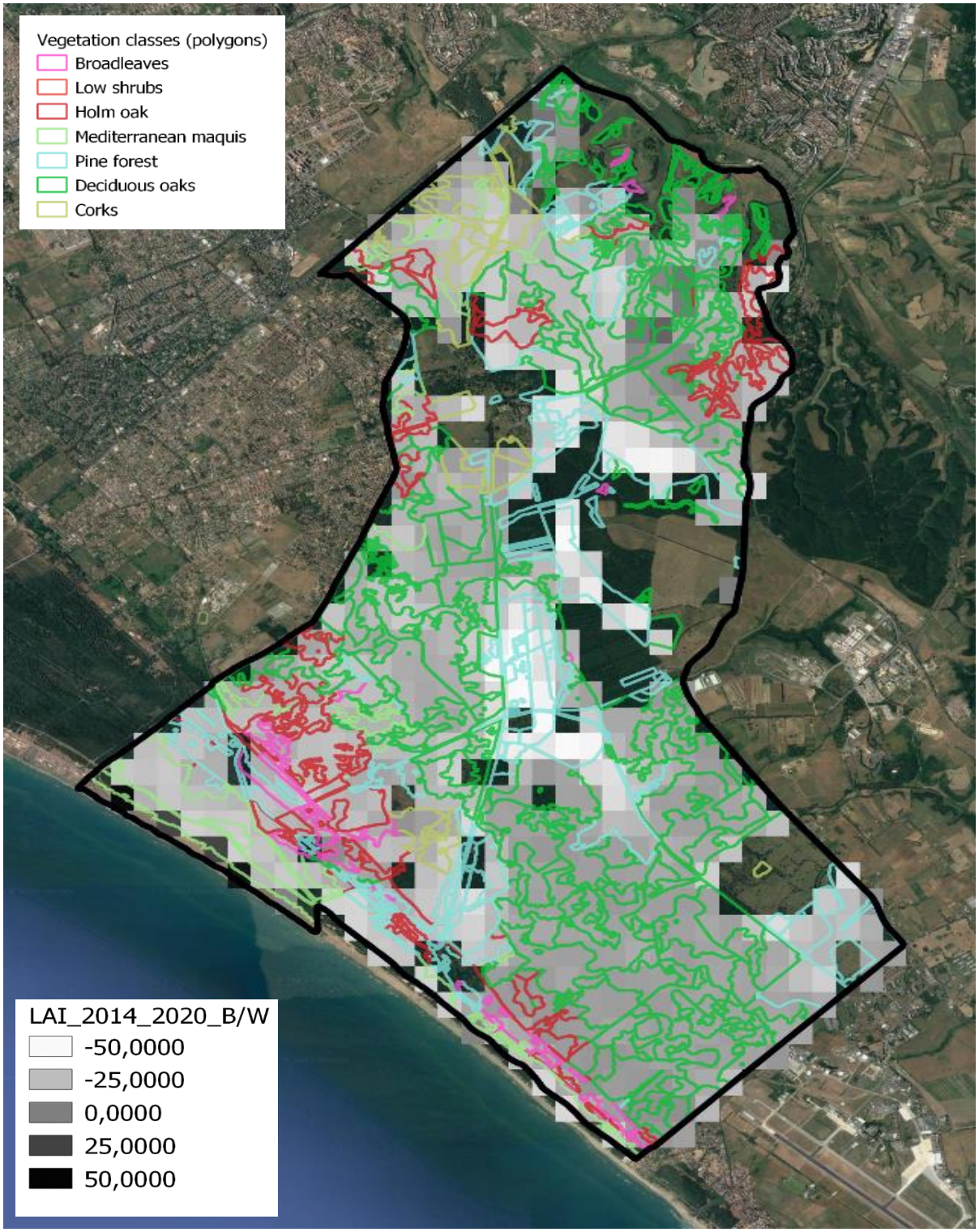

Figure S4. Superimposed maps of vegetation (colored shapes) to LAI (black and white pixels). Colored shapes represent homogeneous groups of vegetation (LCTs). Pixels represents percent change of satellite values of LAI between 2014 and 2020. The vividness of color represent loss or increase of LAI.

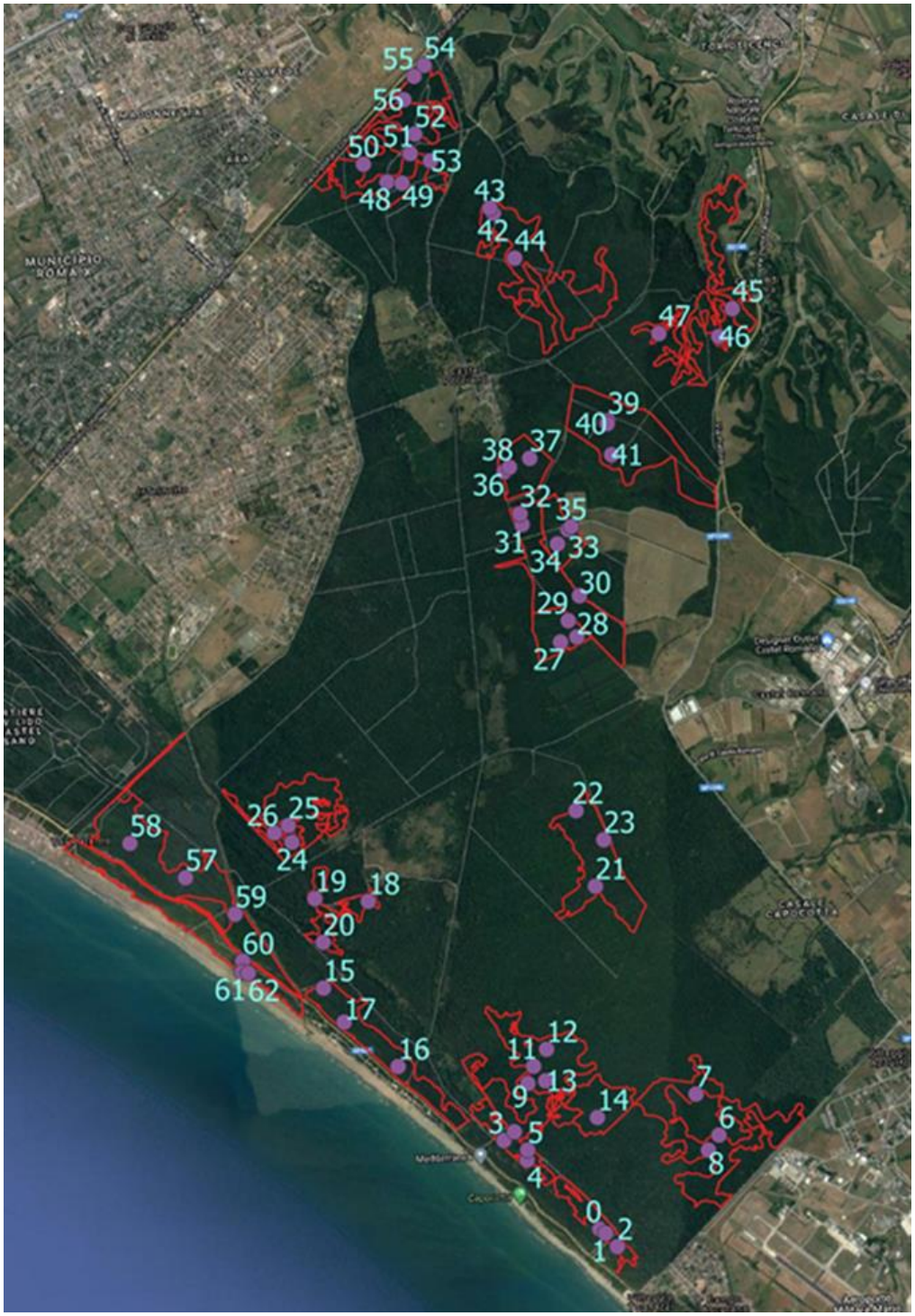

Figure S5. Castelporziano map, showing the sampling points chosen randomly using QGis.

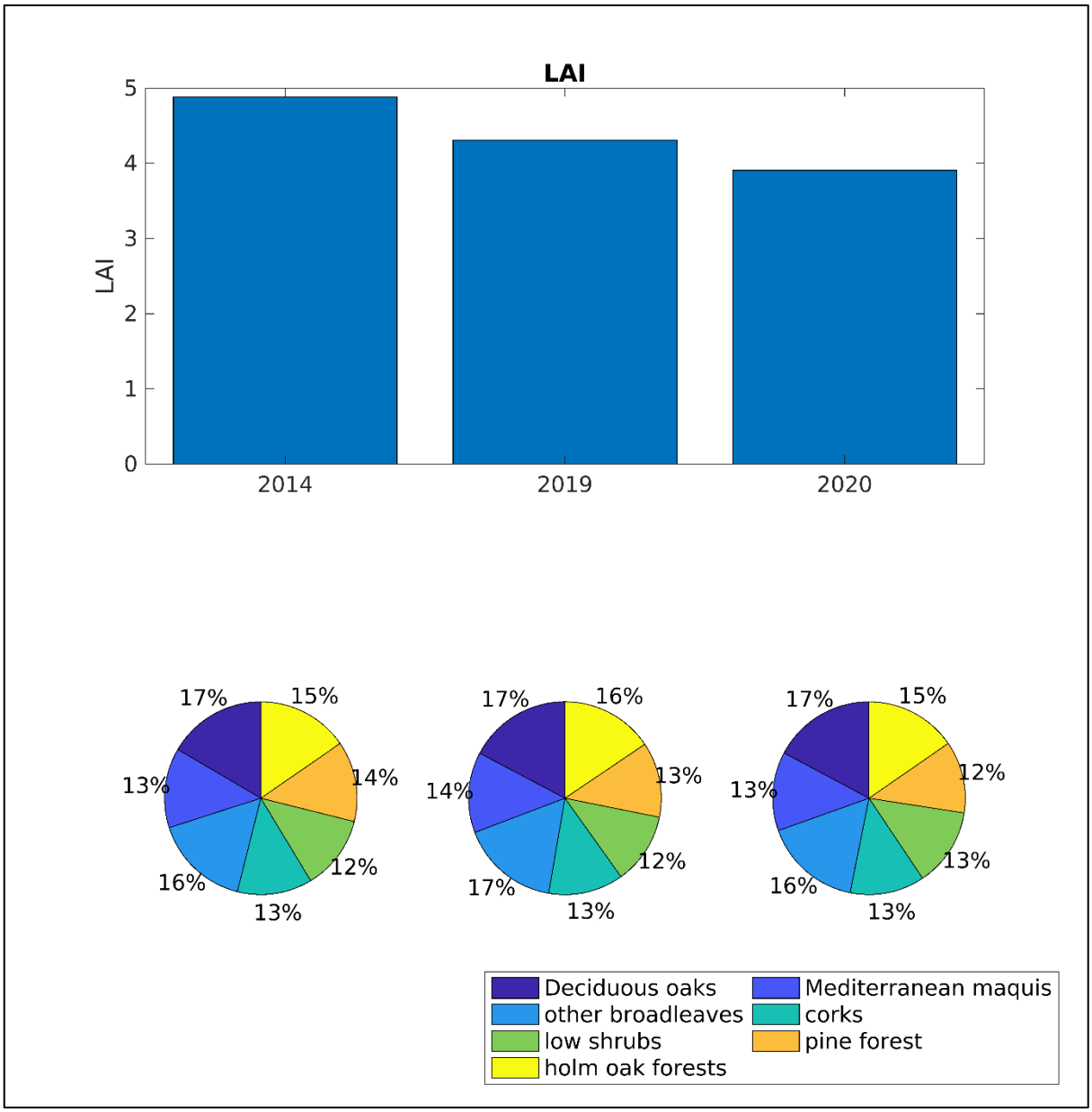

Figure S6. Average values of LAI for the entire Estate of Castelporziano are reported for each of the three years of study (top). Relative contribution to overall LAI by each LCT is shown in pie charts (bottom), for 2014, 2019, and 2020, respectively.

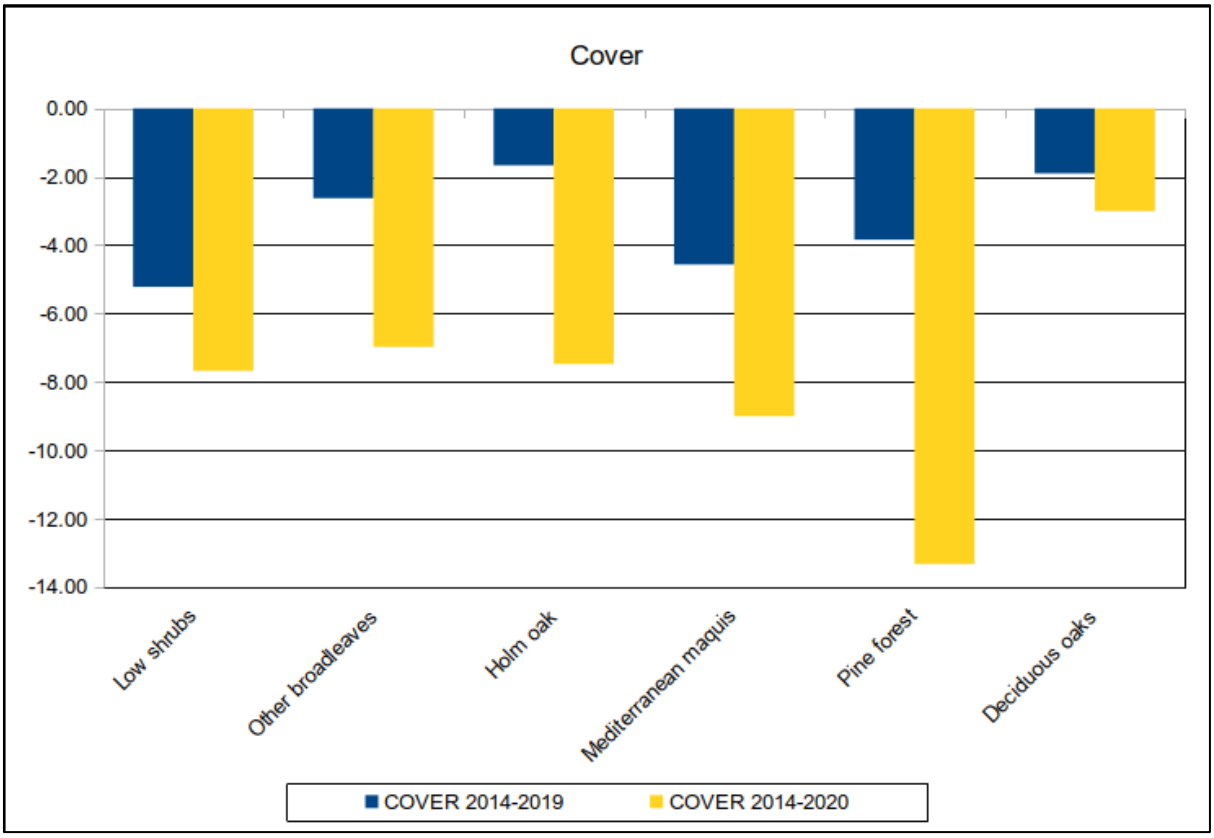

Figure S7. Bar plot showing the percent change of canopy cover values from satellite data between 2014 and 2019, in blue, and 2020 in yellow.

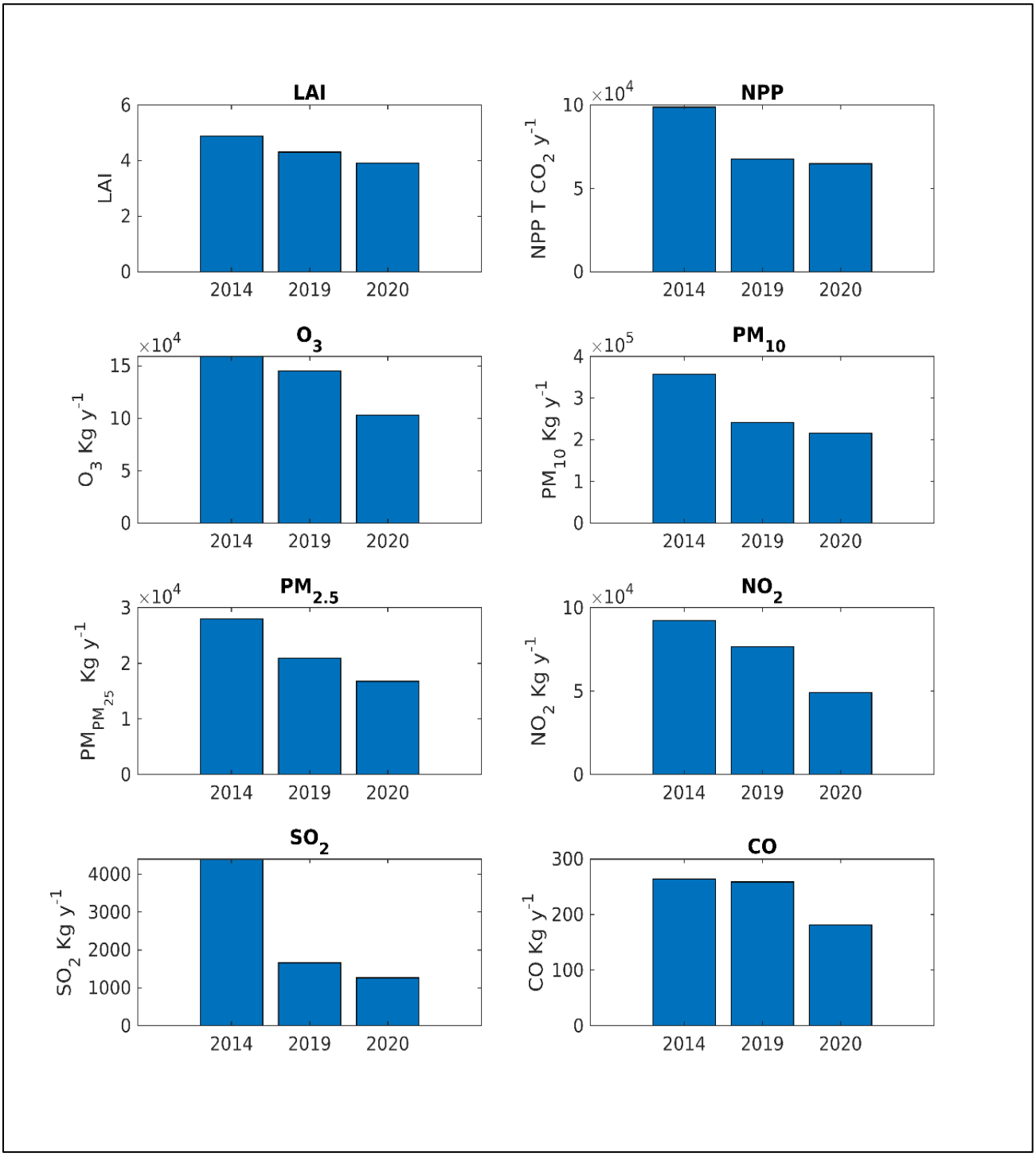

Figure S8. Total estimates of LAI, NPP, and pollutants deposition for the whole Estate in the three years of study.

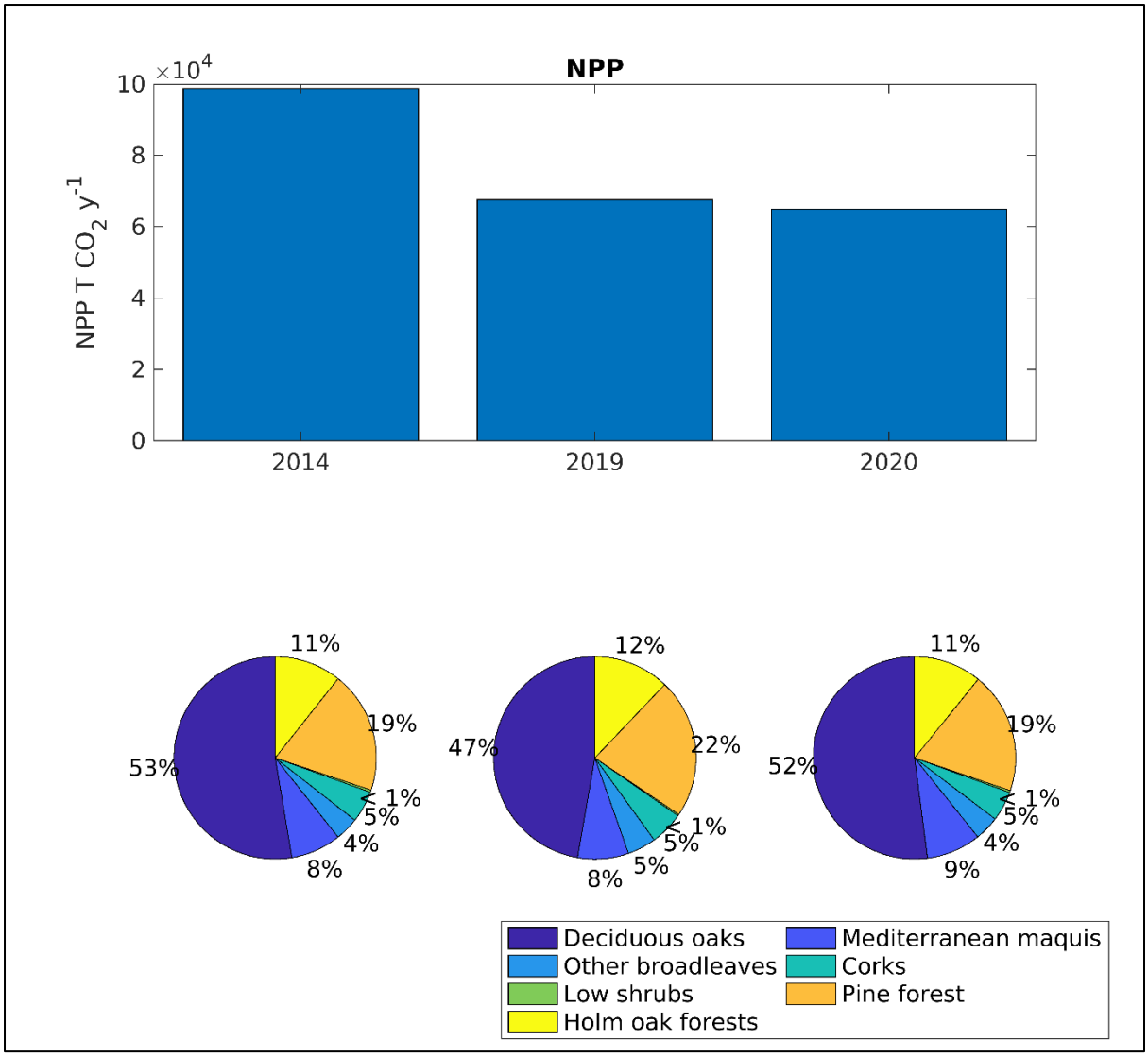

Figure S9. Cumulated values of NPP for the entire Estate of Castelporziano are reported for each of the three years of study (top). Relative contribution to overall NPP by each LCT is shown in pie charts (bottom), for 2014, 2019, and 2020, respectively.

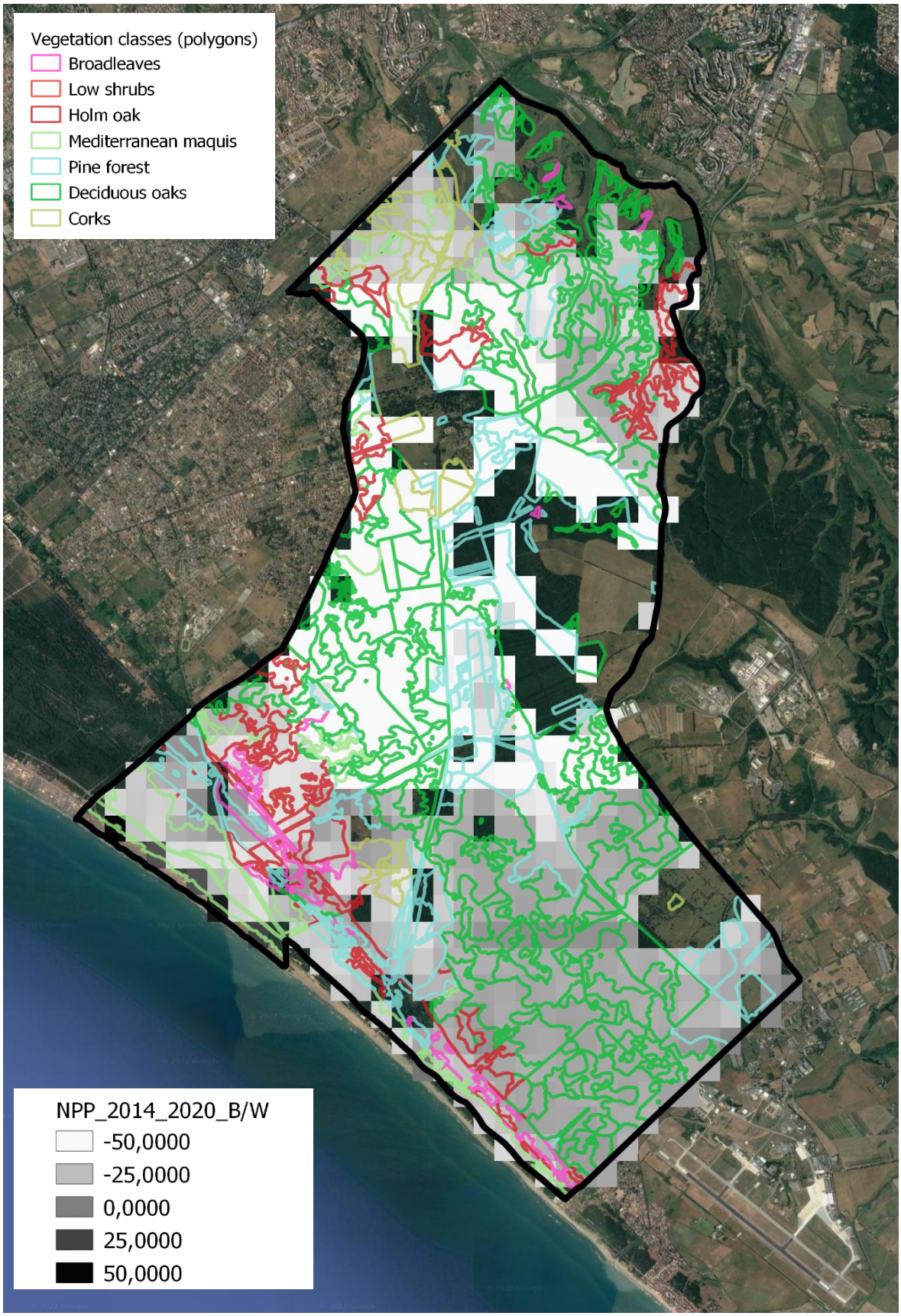
Vegetation classes (polygons)
Broadleaves
Low shrubs
Holm oak
Mediterranean maquis
Pine forest
Deciduous oaks
Corks
NPP_2014_2020_B/W
-50,0000
-25,0000
0,0000
25,0000
50,0000

Figure S10. Superimposed maps of vegetation (colored shapes) to NPP (black and white pixels). Colored shapes represent homogeneous groups of vegetation (LCT). Pixels represents percent change of satellite values of NPP between 2014 and 2020. The vividness of color represent loss or increase of NPP.

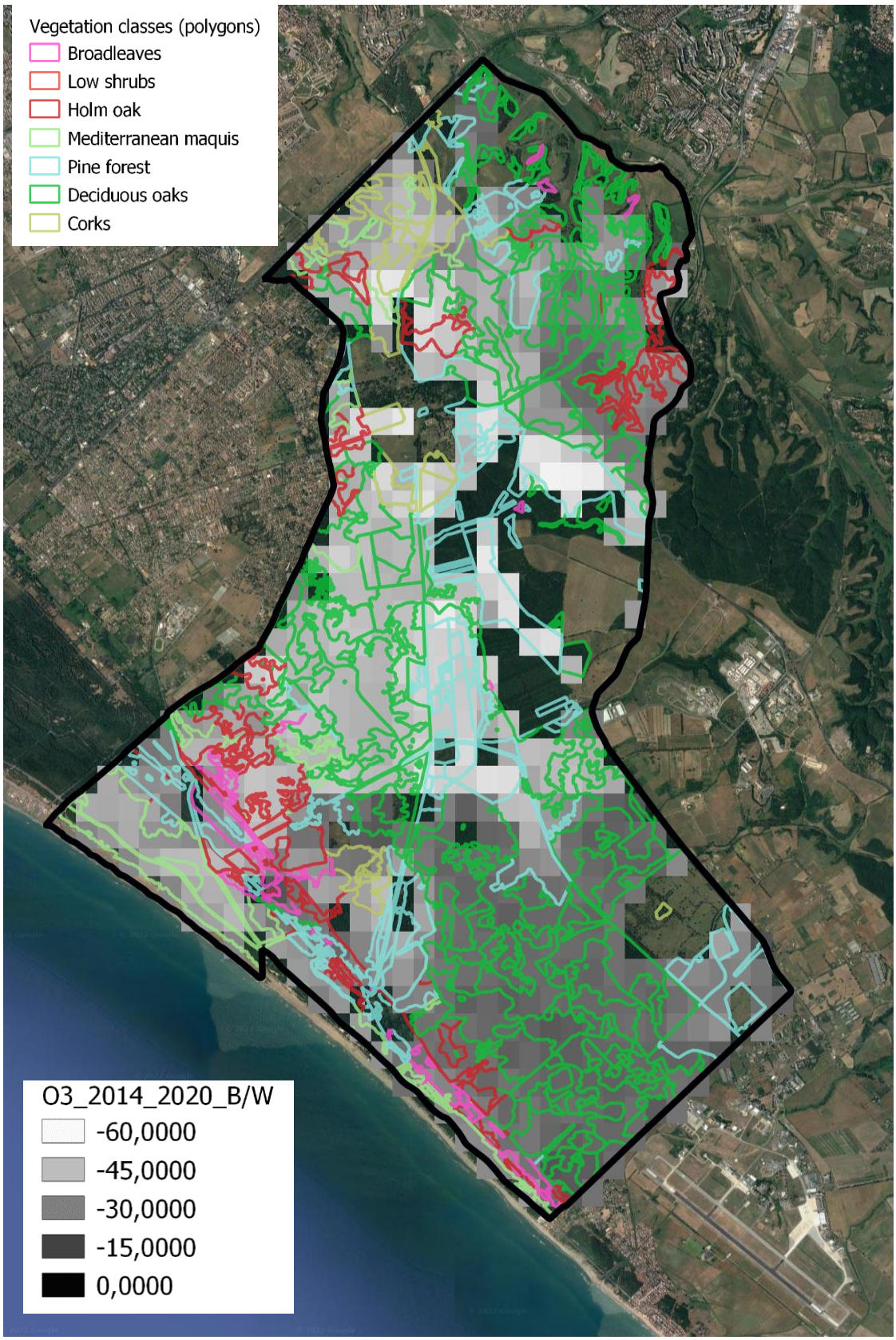

Figure S11. Superimposed maps of vegetation (colored shapes) to O3 fluxes (black and white pixels) . Colored shapes represents homogeneous groups of vegetation (LCTs). Pixels represents percent change of satellite values of O3 fluxes between 2014 and 2020. The vividness of color represent loss or increase of O3 fluxes.

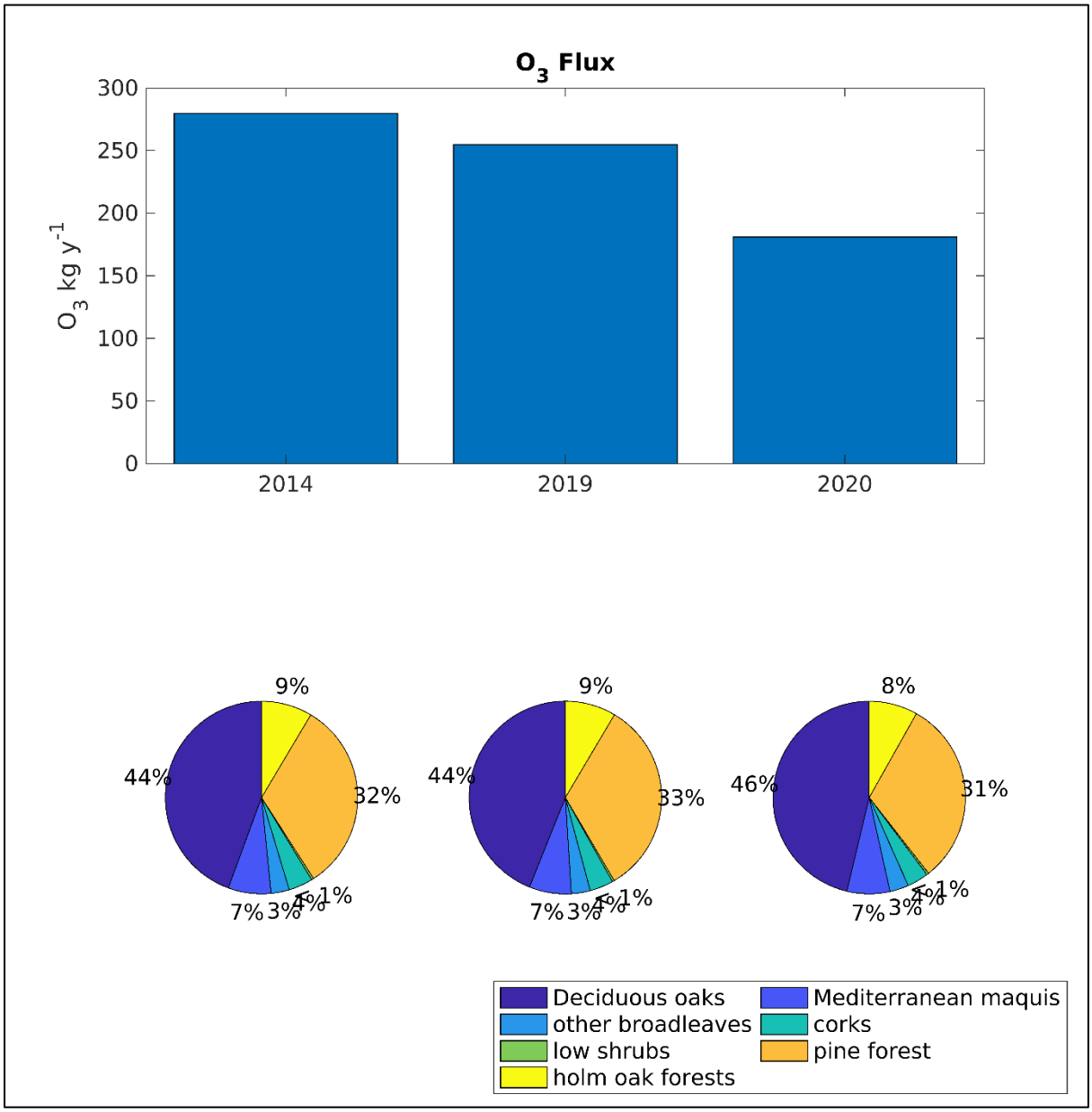

Figure S12. Cumulated values of O3 deposition for the entire Estate of Castelporziano are reported for each of the three years of study (top). Relative contribution to overall O3 deposition by each LCT is shown in pie charts (bottom), for 2014, 2019, and 2020, respectively.

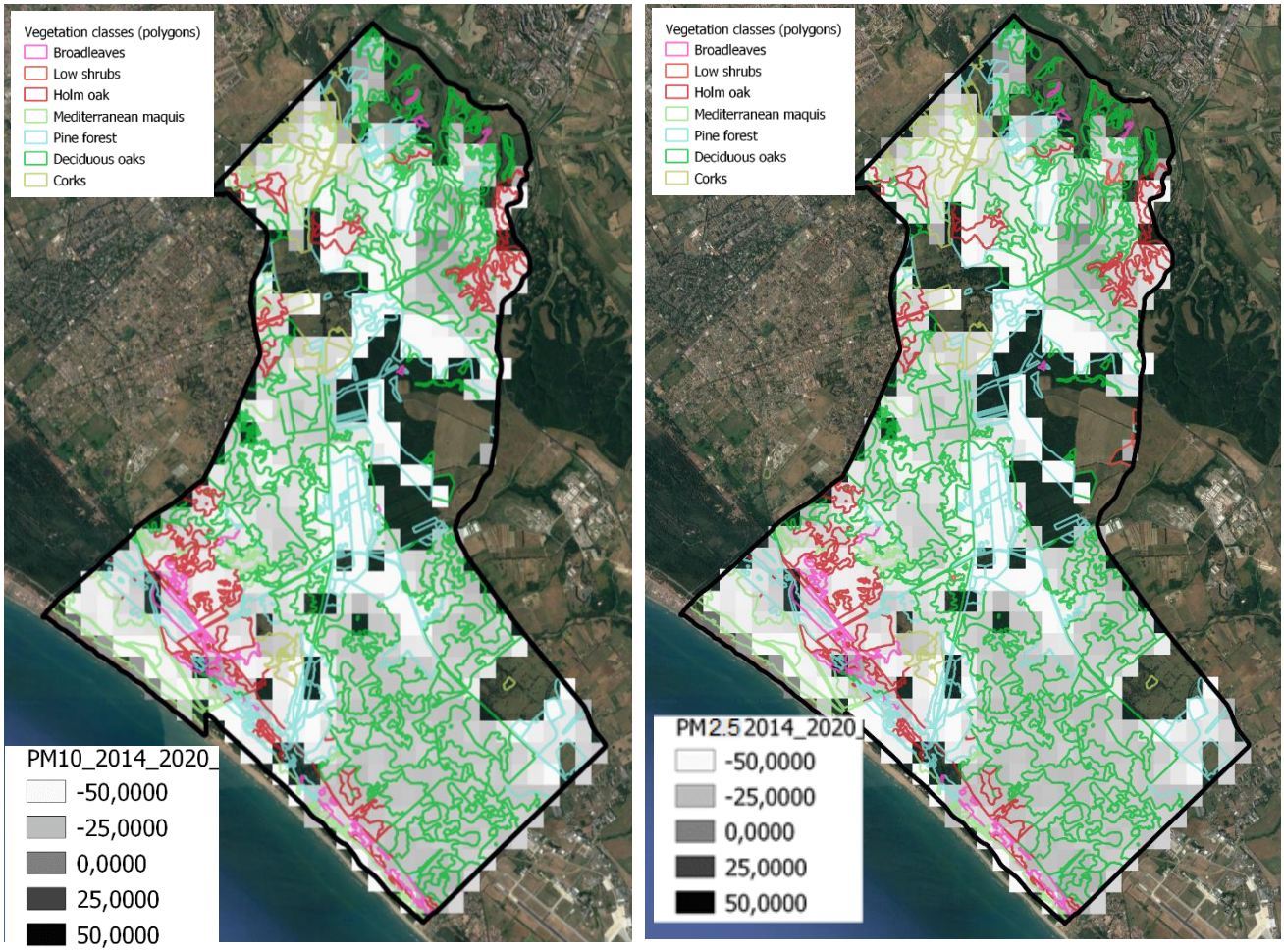

Figure S13. Superimposed maps of vegetation (colored shapes) to PM10 (left) and PM2.5 (right) deposition on canopies (black and white pixels). Colored shapes represent homogeneous groups of vegetation (LCT). Pixels represents percent change of satellite values of LAI between 2014 and 2020. The vividness of color represent loss or increase of LAI.

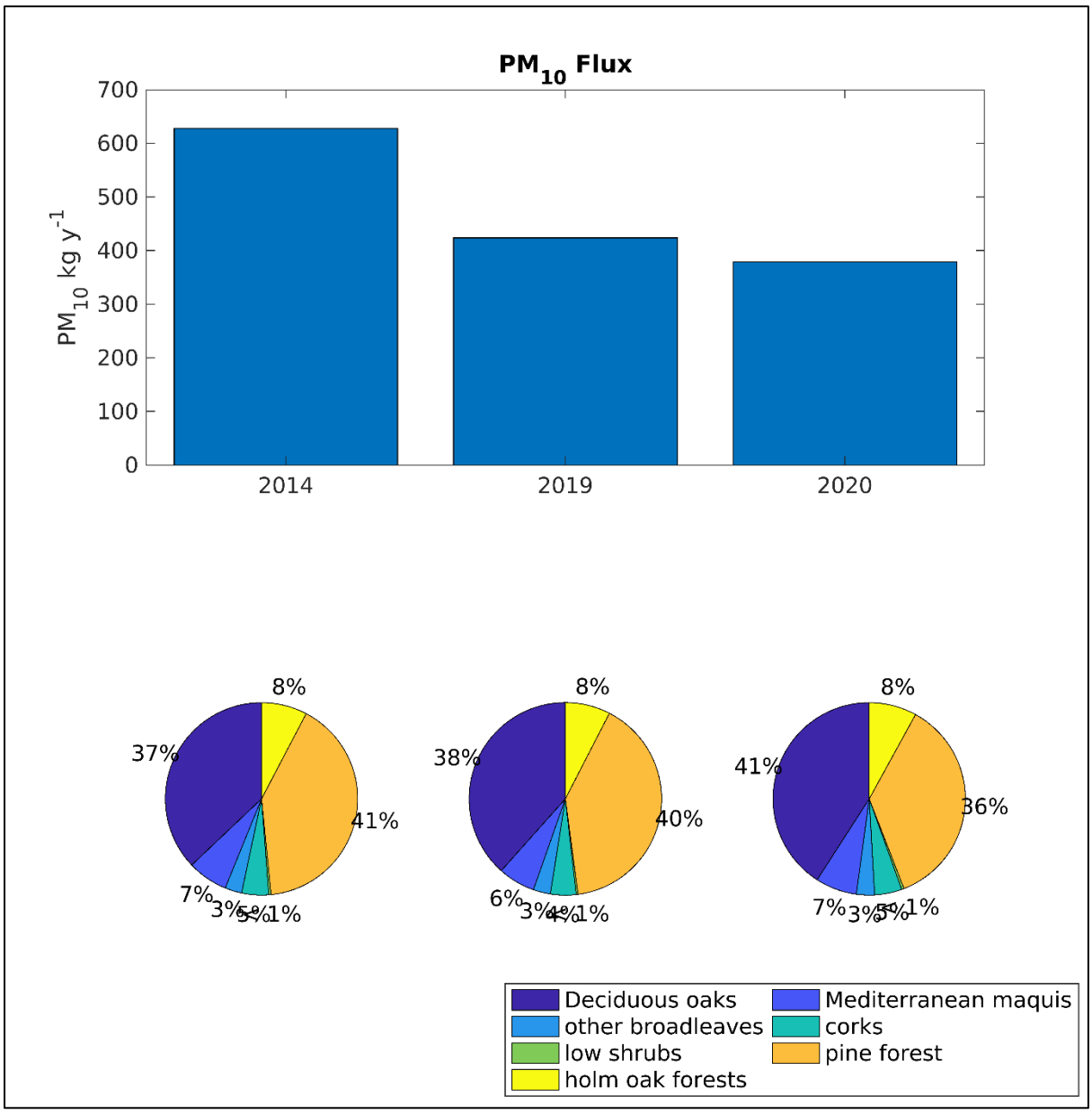

Figure S14. Cumulated values of PM10 deposition for the entire Estate of Castelporziano are reported for each of the three years of study (top). Relative contribution to overall PM10 deposition by each LCT is shown in pie charts (bottom), for 2014, 2019, and 2020, respectively.

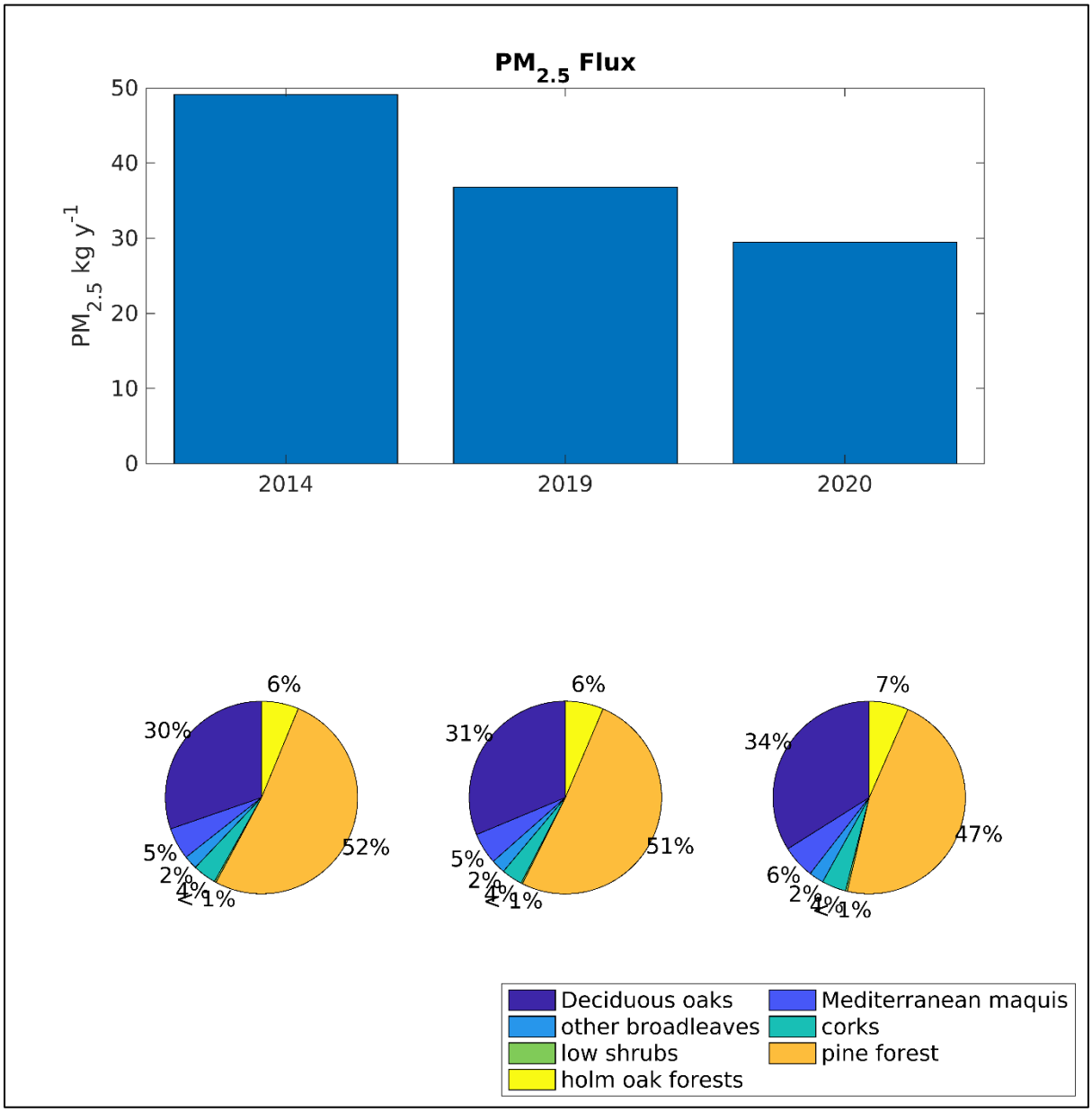

Figure S15. Cumulated values of PM2.5 deposition for the entire Estate of Castelporziano are reported for each of the three years of study (top). Relative contribution to overall PM2.5 deposition by each LCT is shown in pie charts (bottom), for 2014, 2019, and 2020, respectively.

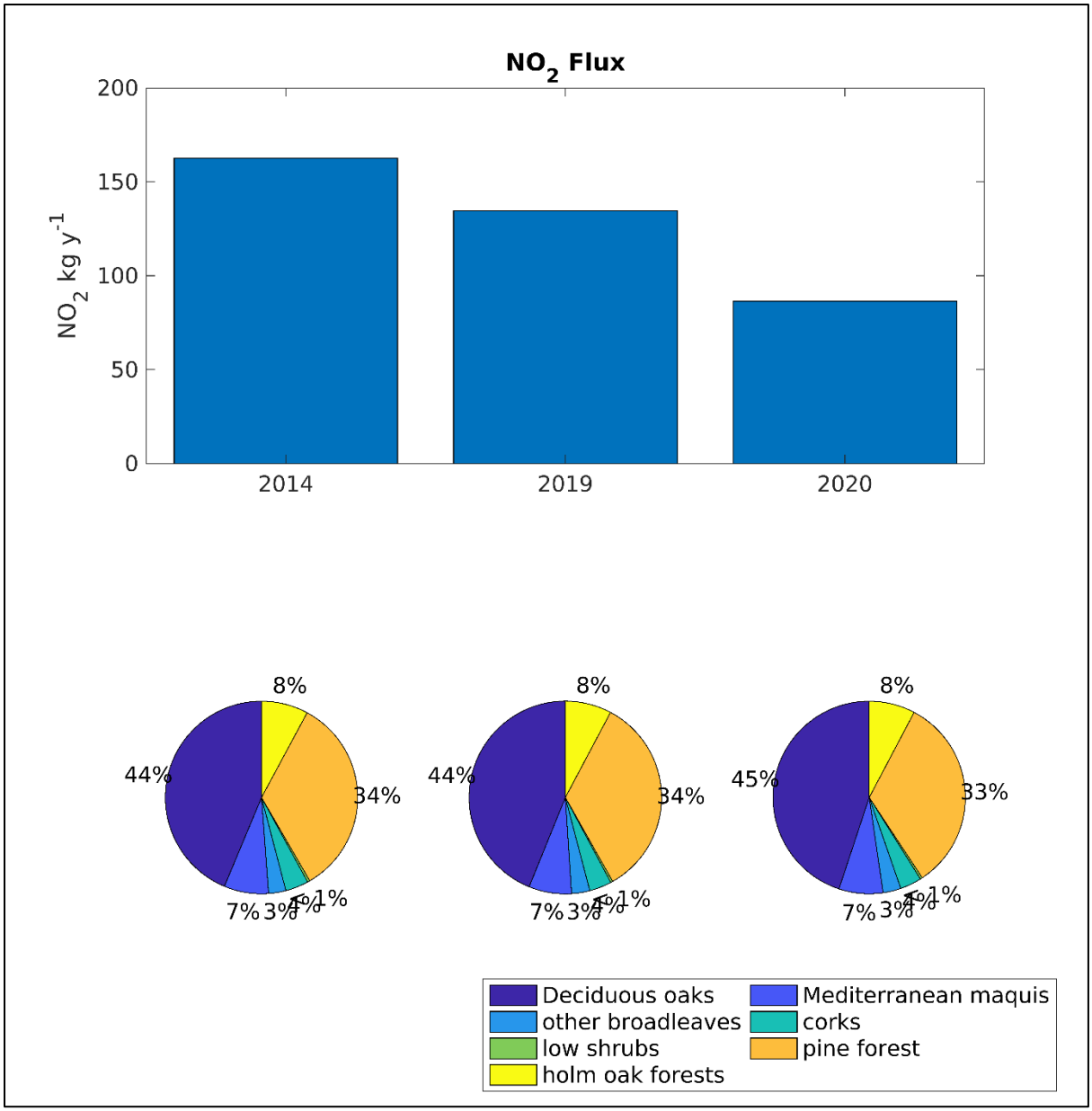

Figure S16. cumulated values of NO2 deposition for the entire Estate of Castelporziano are reported for each of the three years of study (top). Relative contribution to overall NO2 deposition by each LCT is shown in pie charts (bottom), for 2014, 2019, and 2020, respectively.

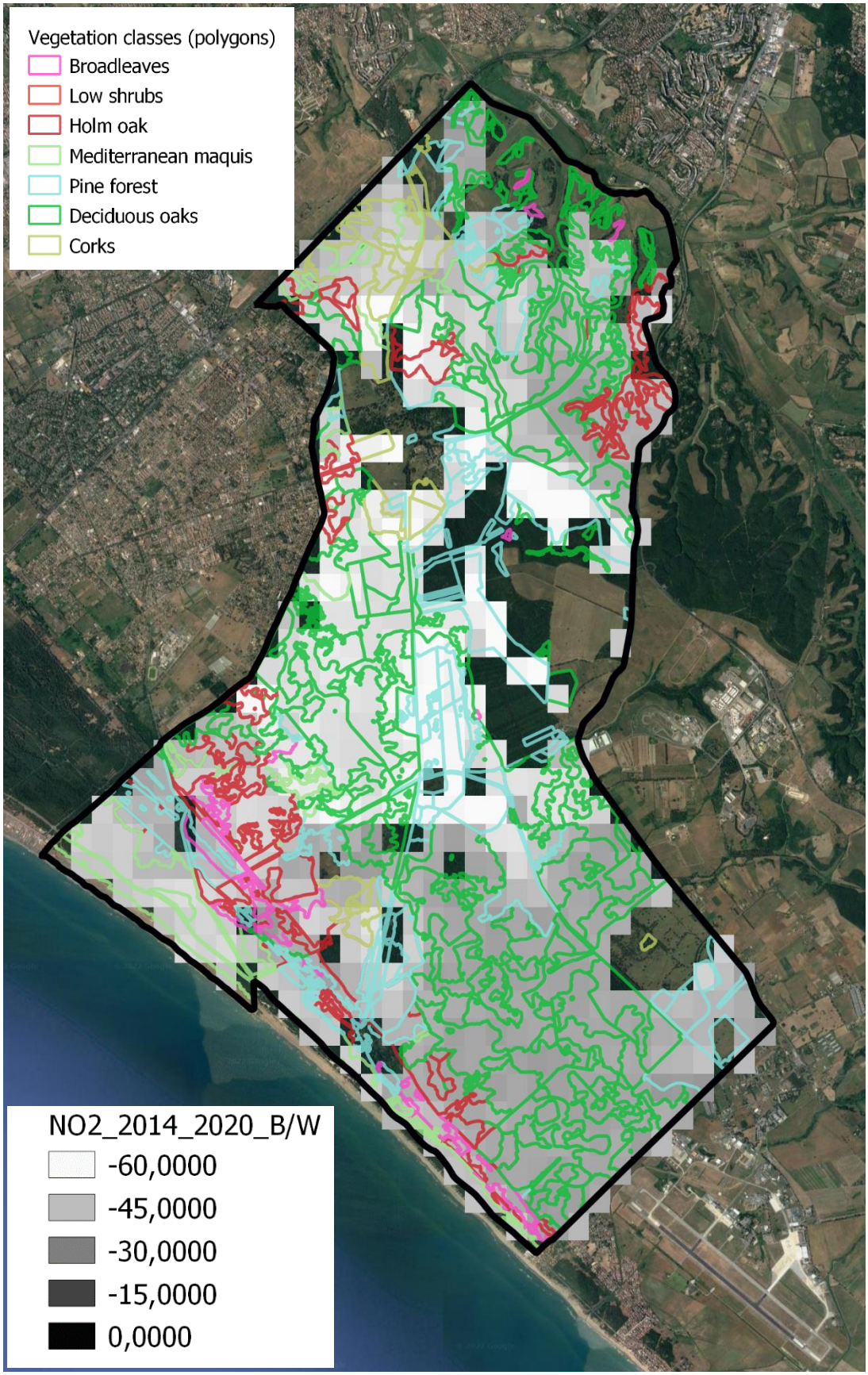

Figure S17. Superimposed maps of vegetation (colored shapes) to NO2 deposition on canopies (black and white pixels). Colored shapes represent homogeneous groups of vegetation (LCT). Pixels represents percent change of satellite values of LAI between 2014 and 2020. The vividness of color represent loss or increase of LAI.

Tables

Table S1. For each LCT, the corresponding association is reported. For each association, average ecophysiological parameters (e.g. Vcmax and ozone tolerance) of the dominant species are used as model input to characterize the LCT ideal tree-type.

LCTs	Association	Dominant species	Vcmax	O3 Tolerance
Mediterranean maquis	*Quercetum ilicis galloprovenzale*	*Pistacia lentiscus L.* *Arbutus unedo L.,* *Juniperus oxycedrus L. ,* *Phillyrea angustifolia L.*	51.8	moderate
Corks	*Quercetum ilicis galloprovenzale suberetosum*	Quercus suber L	61	low
Holm oak forests	-	*Quercus ilex L.,* *Quercus frainetto Ten.,* *Quercus cerris L.,* *Quercus pubescens Willd.* *Fraxinus ornus L.;*	63.5	low
Oak forests	Quercetum ilicis var. farnetto	Quercus cerris L., Quercus frainetto Ten., Carpinus orientalis Mill.	63.5	low
Pine forest	-	Pinus pinea L.	18.7	low
Broadleaves	Hygrophilous woods	*Fraxinus oxycarpa Willd.,* *Alnus glutinosa L.,* *Ulmus minor Mill.,* *Fraxinus ornus L.,* *Ficus carica L.*	71	low
Low shrubs	-	*Rubus ulmifolius Schott.,* *Prunus spinosa L.,* *Crateagus monogyna Jacq.;*	38.6	high

Table S2. LAI, (m2m-2) measured for the different LCTs in Castelporziano Estate. Means accompanied with different letters are significantly different at $p < 0.05$. The difference of LAI between PSVCs was tested by one-way ANOVA followed by post-hoc Student–Neuman–Keuls test at $p \leq 0.05$.

LCTs	Mean ± st. dev.
Holm oak prevailing	4.41 ± 0.62 bc
Mixed deciduous woods	4.12 ± 0.41 b
Pine wood	2.08 ± 0.34 a
Mediterranean maquis	3.85 ± 0.33 b

Table S3. Coefficient of the Fourier model used in this study to simulate LAI at each model time-step. For each LCT, yearly coefficient that best (lowest RMSE) fit LAI measured by satellite data are shown.

LCT	year	a	b	c	d	R^2_{adj}	RMSE
Broadleaves	**2014**	**0,73**	**-0,29**	**-0,01**	**0,02**	**0,94**	**0,05**
	2019	**0,64**	**-0,23**	**0,21**	**0,01**	**0,90**	**0,06**
	2020	**0,67**	**-0,23**	**0,10**	**0,02**	**0,75**	**0,10**
Low shrubs	**2014**	**0,66**	**-0,17**	**0,09**	**0,02**	**0,62**	**0,11**
	2019	**0,63**	**-0,21**	**0,15**	**0,02**	**0,77**	**0,10**
	2020	**0,61**	**-0,20**	**0,16**	**0,02**	**0,67**	**0,12**
Holm oak	**2014**	**0,73**	**-0,29**	**-0,03**	**0,02**	**0,96**	**0,05**

	2019	**0,67**	**-0,28**	**0,10**	**0,02**	**0,91**	**0,06**
	2020	**0,65**	**-0,18**	**0,24**	**0,01**	**0,87**	**0,07**
Mediterranean maquis	**2014**	**0,73**	**-0,26**	**-0,05**	**0,02**	**0,97**	**0,04**
	2019	**0,69**	**-0,27**	**0,03**	**0,02**	**0,92**	**0,06**
	2020	**0,47**	**-0,01**	**0,46**	**0,01**	**0,75**	**0,09**
Deciduous oaks	**2014**	**0,64**	**-0,36**	**0,00**	**0,02**	**0,92**	**0,08**
	2019	**0,63**	**-0,34**	**-0,02**	**0,02**	**0,86**	**0,10**
	2020	**0,53**	**-0,31**	**0,17**	**0,02**	**0,78**	**0,12**
Pine forest	**2014**	**0,76**	**-0,22**	**0,09**	**0,01**	**0,91**	**0,05**
	2019	**0,68**	**-0,19**	**0,20**	**0,01**	**0,88**	**0,06**
	2020	**0,70**	**-0,15**	**0,16**	**0,02**	**0,72**	**0,10**
Corks	**2014**	**0,75**	**-0,22**	**0,05**	**0,02**	**0,95**	**0,03**
	2019	**0,72**	**-0,21**	**0,09**	**0,02**	**0,92**	**0,05**
	2020	**0,77**	**-0,17**	**0,03**	**0,02**	**0,75**	**0,07**

Table S4. Intercomparison between nonlinear models used to fit the day of the year (doy) and LAI of Corks for the year 2014.

Corks				
Model	SSE	R^2	R^2 adj	RMSE
Rational4	0,01	0,97	0,96	0,03
Fourier	0,01	0,96	0,95	0,03
Gauss	0,02	0,94	0,93	0,04
Sin	0,02	0,92	0,91	0,05
Rational5	0,03	0,91	0,88	0,06
Power	0,19	0,30	0,23	0,14
Rational2	0,18	0,36	0,22	0,14
Power2	0,19	0,32	0,17	0,14
Exponential	0,26	0,06	-0,03	0,16
Rational	0,29	-0,04	-0,14	0,17
Exponential2	0,73	-1,64	-2,63	0,30
Weibull	7,26	-25,18	-27,80	0,85
Rational3	7,16	-24,84	-30,58	0,89

Table S5. Intercomparison between nonlinear models used to fit the day of the year (doy) and LAI of Other Broadleaves for the year 2014.

Other broadleaves				
Model	SSE	R^2	R^2 adj	RMSE
Fourier	0,02	0,96	0,94	0,05
Rational4	0,02	0,95	0,94	0,06
Gauss	0,04	0,93	0,91	0,07
Sin	0,06	0,89	0,86	0,08
Rational5	0,07	0,86	0,81	0,10
Power	0,41	0,21	0,13	0,20
Rational2	0,38	0,28	0,12	0,21
Power2	0,40	0,23	0,06	0,21
Exponential	0,51	0,03	-0,07	0,23
Rational	0,53	-0,02	-0,12	0,23

Exponential2	0,65	-0,24	-0,70	0,28
Weibull	6,62	-11,65	-12,91	0,81
Rational3	6,56	-11,54	-14,33	0,85

Table S6. Intercomparison between nonlinear models used to fit the day of the year (doy) and LAI of Deciduous Oaks for the year 2014.

Deciduous oaks				
Model	SSE	R^2	R^2 adj	RMSE
Fourier	0,05	0,94	0,92	0,08
Gauss	0,06	0,93	0,91	0,08
Sin	0,10	0,88	0,85	0,11
Rational5	0,12	0,85	0,79	0,12
Power	0,63	0,21	0,14	0,25
Rational2	0,58	0,28	0,12	0,25
Power2	0,62	0,23	0,06	0,26
Exponential	0,78	0,03	-0,06	0,28
Rational	0,82	-0,01	-0,11	0,29
Exponential2	0,99	-0,22	-0,68	0,35
Weibull	5,71	-6,06	-6,77	0,76
Rational3	5,68	-6,03	-7,59	0,79
Rational4	5,64	-5,98	-8,59	0,84

Table S7. Intercomparison between nonlinear models used to fit the day of the year (doy) and LAI of Holm oak forest for the year 2014.

Holm oak forest				
Model	SSE	R^2	R^2 adj	RMSE
Fourier	0,02	0,97	0,96	0,05
Gauss	0,03	0,94	0,92	0,06
Sin	0,06	0,89	0,87	0,08
Rational5	0,07	0,87	0,82	0,09
Exponential2	0,11	0,80	0,72	0,12
Power	0,41	0,24	0,17	0,20
Rational2	0,38	0,31	0,15	0,20
Power2	0,40	0,25	0,09	0,21
Exponential	0,52	0,05	-0,05	0,23
Rational	0,55	-0,02	-0,12	0,24
Weibull	6,61	-11,21	-12,44	0,81
Rational3	6,56	-11,12	-13,81	0,85
Rational4	6,38	-10,79	-15,21	0,89

Table S8. Intercomparison between nonlinear models used to fit the day of the year (doy) and LAI of Mediterranean maquis for the year 2014.

Mediterranean maquis				
Model	SSE	R^2	R^2 adj	RMSE

Fourier	0,01	0,97	0,97	0,04
Gauss	0,03	0,93	0,91	0,06
Sin	0,05	0,88	0,86	0,08
Power	0,33	0,25	0,18	0,18
Rational2	0,31	0,31	0,16	0,18
Power2	0,33	0,26	0,09	0,19
Rational5	0,34	0,25	-0,04	0,21
Exponential	0,42	0,06	-0,04	0,21
Rational	0,46	-0,03	-0,13	0,21
Exponential2	0,60	-0,33	-0,83	0,27
Weibull	6,57	-13,70	-15,16	0,81
Rational3	6,49	-13,51	-16,74	0,85
Rational4	6,50	-13,54	-18,99	0,90

Table S9. Intercomparison between nonlinear models used to fit the day of the year (doy) and LAI of Pine forest for the year 2014.

Pine forest				
Model	SSE	R^2	R^2 adj	RMSE
Rational3	0,02	0,93	0,92	0,05
Fourier	0,02	0,94	0,91	0,05
Rational4	0,02	0,93	0,91	0,05
Gauss	0,02	0,92	0,91	0,05
Sin	0,03	0,90	0,88	0,06
Rational5	0,04	0,88	0,83	0,07
Exponential2	0,07	0,77	0,68	0,09
Power	0,20	0,33	0,26	0,14
Rational2	0,18	0,39	0,26	0,14
Power2	0,20	0,34	0,19	0,15
Exponential	0,27	0,08	-0,01	0,17
Rational	0,31	-0,03	-0,13	0,18
Weibull	7,76	-24,88	-27,47	0,88

Table S10. Intercomparison between nonlinear models used to fit the day of the year (doy) and LAI of Low shrubs for the year 2014.

Low shrubs				
Model	SSE	R^2	R^2 adj	RMSE
Fourier	0,09	0,72	0,62	0,11
Rational3	0,11	0,66	0,58	0,11
Exponential2	0,10	0,69	0,57	0,11
Rational5	0,11	0,67	0,55	0,12
Gauss	0,12	0,62	0,54	0,12
Sin	0,13	0,59	0,50	0,12
Power	0,31	0,05	-0,05	0,18
Rational2	0,28	0,13	-0,06	0,18
Power2	0,28	0,13	-0,06	0,18
Exponential	0,31	0,03	-0,06	0,18
Rational	0,32	0,03	-0,07	0,18
Weibull	5,04	-14,53	-16,08	0,71

Rational4	5,01	-14,45	-20,24	0,79

Table S11. Intercomparison between nonlinear models used to fit the day of the year (doy) and LAI of Other broadleaves for the year 2019.

Other broadleaves				
Model	SSE	R^2	R^2 adj	RMSE
Gauss	0,03	0,93	0,91	0,06
Rational3	0,03	0,92	0,91	0,06
Fourier	0,03	0,93	0,90	0,06
Sin	0,04	0,92	0,90	0,06
Rational5	0,04	0,90	0,86	0,07
Power	0,35	0,20	0,12	0,19
Rational2	0,32	0,27	0,11	0,19
Power2	0,34	0,24	0,07	0,19
Exponential	0,43	0,01	-0,08	0,21
Rational	0,45	-0,01	-0,12	0,21
Exponential2	1,33	-2,02	-3,16	0,41
Weibull	6,42	-13,60	-15,06	0,80
Rational4	6,25	-13,21	-18,54	0,88

Table S12. Intercomparison between nonlinear models used to fit the day of the year (doy) and LAI of Corks for the year 2019.

Corks				
Model	SSE	R^2	R^2 adj	RMSE
Fourier	0,02	0,94	0,92	0,05
Gauss	0,02	0,93	0,91	0,05
Sin	0,03	0,91	0,89	0,05
Rational5	0,03	0,90	0,86	0,06
Exponential2	0,08	0,73	0,63	0,10
Power	0,24	0,18	0,10	0,16
Rational2	0,22	0,24	0,08	0,16
Power2	0,23	0,21	0,03	0,16
Exponential	0,29	0,01	-0,09	0,17
Rational	0,30	-0,02	-0,12	0,17
Weibull	6,65	-21,64	-23,90	0,82
Rational3	6,58	-21,40	-26,38	0,86
Rational4	6,59	-21,42	-29,82	0,91

Table S13. Intercomparison between nonlinear models used to fit the day of the year (doy) and LAI of Deciduous oaks for the year 2019.

Deciduous oaks				
Model	SSE	R^2	R^2 adj	RMSE
Fourier	0,08	0,90	0,86	0,10
Gauss	0,09	0,88	0,86	0,10

Sin	0,13	0,83	0,80	0,12
Power	0,64	0,18	0,10	0,25
Power2	0,63	0,19	0,01	0,26
Rational2	0,68	0,12	-0,07	0,28
Exponential	0,76	0,02	-0,08	0,28
Rational	0,79	-0,01	-0,11	0,28
Rational5	0,68	0,12	-0,21	0,29
Exponential2	1,15	-0,48	-1,04	0,38
Weibull	5,27	-5,77	-6,45	0,73
Rational3	5,24	-5,73	-7,23	0,76
Rational4	5,09	-5,54	-7,99	0,80

Table S14– Intercomparison between nonlinear models used to fit the day of the year (doy) and LAI of Holm oak forest for the year 2019.

Holm oak forest				
Model	SSE	R^2	R^2 adj	RMSE
Fourier	0,03	0,94	0,91	0,06
Gauss	0,04	0,93	0,91	0,06
Sin	0,05	0,91	0,89	0,07
Rational5	0,06	0,88	0,83	0,09
Exponential2	0,16	0,69	0,57	0,14
Power	0,39	0,21	0,13	0,20
Rational2	0,36	0,27	0,11	0,20
Power2	0,38	0,23	0,06	0,21
Exponential	0,49	0,02	-0,08	0,22
Rational	0,50	-0,01	-0,12	0,22
Weibull	6,23	-11,53	-12,78	0,79
Rational3	6,15	-11,38	-14,13	0,83
Rational4	6,16	-11,40	-16,05	0,88

Table S15. Intercomparison between nonlinear models used to fit the day of the year (doy) and LAI of Mediterranean maquis for the year 2019.

Mediterranean maquis				
Model	SSE	R^2	R^2 adj	RMSE
Fourier	0,03	0,94	0,92	0,06
Gauss	0,03	0,92	0,90	0,06
Sin	0,05	0,89	0,87	0,07
Rational5	0,06	0,86	0,81	0,09
Power	0,35	0,21	0,13	0,19
Rational2	0,33	0,27	0,11	0,19
Power2	0,35	0,23	0,06	0,20
Exponential	0,44	0,03	-0,07	0,21
Rational	0,46	-0,02	-0,12	0,21
Exponential2	0,53	-0,19	-0,63	0,26
Weibull	6,20	-12,85	-14,23	0,79
Rational3	6,13	-12,68	-15,72	0,83

Rational4	6,12	-12,67	-17,79	0,87

Table S16. Intercomparison between nonlinear models used to fit the day of the year (doy) and LAI of Pine forest for the year 2019.

Pine forest				
Model	SSE	R^2	R^2 adj	RMSE
Gauss	0,03	0,91	0,89	0,06
Fourier	0,03	0,91	0,88	0,06
Sin	0,04	0,90	0,88	0,06
Rational5	0,04	0,89	0,85	0,07
Power	0,32	0,11	0,02	0,18
Power2	0,30	0,16	-0,03	0,18
Rational2	0,32	0,11	-0,09	0,19
Exponential	0,36	0,00	-0,10	0,19
Rational	0,36	0,00	-0,10	0,19
Exponential2	1,49	-3,19	-4,76	0,43
Weibull	6,65	-17,65	-19,52	0,82
Rational3	6,58	-17,45	-21,55	0,85
Rational4	6,52	-17,29	-24,14	0,90

Table S17. Intercomparison between nonlinear models used to fit the day of the year (doy) and LAI of Low shrubs for the year 2019.

Low shrubs				
Model	SSE	R^2	R^2 adj	RMSE
Rational4	0,06	0,86	0,81	0,09
Gauss	0,08	0,83	0,79	0,09
Fourier	0,07	0,83	0,77	0,10
Sin	0,09	0,81	0,76	0,10
Exponential2	0,13	0,70	0,59	0,13
Power	0,42	0,07	-0,02	0,20
Power2	0,39	0,13	-0,07	0,21
Exponential	0,44	0,01	-0,09	0,21
Rational	0,44	0,01	-0,09	0,21
Rational2	0,40	0,10	-0,10	0,21
Rational5	0,38	0,16	-0,16	0,22
Weibull	5,30	-10,84	-12,03	0,73
Rational3	5,25	-10,72	-13,32	0,76

Table S18. Intercomparison between nonlinear models used to fit the day of the year (doy) and LAI of Other broadleaves for the year 2020.

Other broadleaves				
Model	SSE	R^2	R^2 adj	RMSE
Gauss	0,09	0,81	0,76	0,10

Fourier	0,08	0,82	0,75	0,10
Sin	0,10	0,79	0,74	0,10
Rational5	0,09	0,81	0,74	0,10
Exponential2	0,11	0,77	0,68	0,11
Rational2	0,35	0,23	0,05	0,20
Power	0,39	0,14	0,05	0,20
Power2	0,36	0,21	0,03	0,20
Exponential	0,46	0,00	-0,10	0,21
Rational	0,46	0,00	-0,10	0,21
Weibull	5,61	-11,32	-12,55	0,75
Rational3	5,56	-11,22	-13,93	0,79
Rational4	5,56	-11,22	-15,81	0,83

Table S19. Intercomparison between nonlinear models used to fit the day of the year (doy) and LAI of Corks for the year 2020.

Corks				
Model	SSE	R^2	R^2 adj	RMSE
Fourier	0,04	0,82	0,75	0,07
Rational3	0,05	0,76	0,70	0,08
Gauss	0,06	0,73	0,67	0,08
Exponential2	0,05	0,75	0,66	0,08
Rational5	0,05	0,75	0,66	0,08
Sin	0,06	0,72	0,65	0,08
Power	0,20	0,11	0,02	0,14
Rational2	0,18	0,18	0,00	0,14
Power2	0,18	0,17	-0,01	0,14
Exponential	0,22	0,00	-0,09	0,15
Rational	0,22	0,00	-0,10	0,15
Weibull	6,56	-28,83	-31,81	0,81
Rational4	6,40	-28,11	-39,03	0,89

Table S20. Intercomparison between nonlinear models used to fit the day of the year (doy) and LAI of Deciduous oaks for the year 2020.

Deciduous oaks				
Model	SSE	R^2	R^2 adj	RMSE
Gauss	0,12	0,84	0,80	0,12
Fourier	0,12	0,84	0,78	0,12
Sin	0,14	0,82	0,78	0,12
Rational5	0,15	0,81	0,74	0,14
Exponential2	0,27	0,64	0,51	0,18
Power	0,67	0,13	0,04	0,26
Power2	0,64	0,16	-0,02	0,27
Rational2	0,66	0,13	-0,06	0,27
Exponential	0,76	0,00	-0,10	0,28
Rational	0,77	0,00	-0,11	0,28
Weibull	4,57	-4,98	-5,58	0,68

Rational3	4,54	-4,95	-6,28	0,71
Rational4	4,53	-4,93	-7,15	0,75

Table S21. Intercomparison between nonlinear models used to fit the day of the year (doy) and LAI of Holm oak forest for the year 2020.

Holm oak forest				
Model	SSE	R^2	R^2 adj	RMSE
Gauss	0,04	0,90	0,88	0,07
Rational3	0,04	0,90	0,88	0,07
Sin	0,04	0,90	0,87	0,07
Fourier	0,04	0,91	0,87	0,07
Rational5	0,04	0,90	0,87	0,07
Exponential2	0,07	0,83	0,76	0,09
Rational2	0,32	0,22	0,05	0,19
Power	0,36	0,13	0,04	0,19
Power2	0,33	0,20	0,03	0,19
Exponential	0,41	0,00	-0,10	0,20
Rational	0,41	0,00	-0,10	0,20
Weibull	6,52	-14,96	-16,56	0,81
Rational4	6,46	-14,81	-20,74	0,90

Table S22. Intercomparison between nonlinear models used to fit the day of the year (doy) and LAI of Mediterranean maquis for the year 2020.

Mediterranean maquis				
Model	SSE	R^2	R^2 adj	RMSE
Gauss	0,07	0,82	0,78	0,09
Sin	0,07	0,82	0,78	0,09
Rational5	0,07	0,83	0,77	0,09
Fourier	0,07	0,82	0,75	0,09
Exponential2	0,09	0,77	0,68	0,11
Power	0,35	0,13	0,04	0,19
Rational2	0,31	0,22	0,04	0,19
Power2	0,32	0,20	0,03	0,19
Exponential	0,40	0,00	-0,10	0,20
Rational	0,40	0,00	-0,10	0,20
Weibull	6,45	-15,16	-16,78	0,80
Rational3	6,37	-14,95	-18,49	0,84
Rational4	6,33	-14,84	-20,79	0,89

Table S23. Intercomparison between nonlinear models used to fit the day of the year (doy) and LAI of Pine forest for the year 2020.

Pine forest				
Model	SSE	R^2	R^2 adj	RMSE

Fourier	0,07	0,80	0,72	0,10
Exponential2	0,09	0,75	0,66	0,11
Rational3	0,11	0,69	0,63	0,11
Rational5	0,11	0,71	0,60	0,12
Gauss	0,14	0,62	0,54	0,12
Sin	0,15	0,57	0,48	0,13
Exponential	0,31	0,13	0,05	0,18
Rational	0,32	0,12	0,03	0,18
Power	0,36	0,01	-0,09	0,19
Rational2	0,33	0,10	-0,10	0,19
Power2	0,33	0,09	-0,12	0,19
Weibull	5,72	-14,76	-16,33	0,76
Rational4	5,63	-14,53	-20,35	0,84

Table S24. Intercomparison between nonlinear models used to fit the day of the year (doy) and LAI of Low shrubs for the year 2020.

Low shrubs				
Model	SSE	R^2	R^2 adj	RMSE
Fourier	0,12	0,76	0,67	0,12
Exponential2	0,13	0,74	0,64	0,13
Rational5	0,16	0,70	0,58	0,14
Gauss	0,20	0,62	0,53	0,15
Sin	0,23	0,56	0,46	0,16
Exponential	0,48	0,07	-0,02	0,22
Rational	0,48	0,06	-0,04	0,22
Power2	0,45	0,13	-0,07	0,22
Power	0,50	0,03	-0,07	0,22
Rational2	0,47	0,08	-0,12	0,23
Weibull	4,52	-7,83	-8,71	0,67
Rational3	4,47	-7,73	-9,67	0,70
Rational4	4,40	-7,61	-10,83	0,74

Appendix A

In situ LAI measurements

We decided to carry out the comparison with satellite measurements by comparing field data collected through two methods based on multiple simultaneous measurements of transmittance (indirect optical methods): the use of the LAI-2200C Plant Canopy Analyzer by Li-Cor instrument and the use of hemispherical photography. Leaf Area Index (LAI, m2m-2) was measured using a LAI-2200 Plant Canopy Analyzer (Li-Cor, Lincoln, NE, USA) which measures simultaneously diffuse radiation through a fisheye light sensor composed by five angular bands with angle of 7°, 23°, 38°, 53° and 68°. The LAI is estimated by the calculation of the "gap fraction" starting from measurements outside the stand (A readings) and below the canopy (B readings) and then calculating the differences between the incident radiation without and below the canopy. The A measures were recorded in open areas close to the experimental sites at the beginning and at the end of each measurement cycle to minimize the effect that change in the light conditions during the measurements, can have on data. The B measurements, carried out by applying a 90° view cup on the lens, were carried out in each sampling point using a regular scheme that includes, for each of the three measures, four replicates that were recorded at a regular distance, including at the vertices of a square. The sampling points were selected through a stratified sampling procedure developed in a GIS environment (Figure S6). Starting from the vegetation map provided by Recanatesi (2015), four Physiognomic Structural Vegetation Categories (PSVCs) were selected for LAI field measures: Mediterranean maquis, Mixed deciduous woods, pine wood, Holm oak prevailing stand. For each category, 3 polygons were chosen randomly by the GIS and a representative sampling point was selected in each of these polygons. Measurements were taken during an intensive field campaign carried out in September 2021, from 6th to 10th, during successive days of stable and comparable weather conditions. The measurements were taken during the day using a scattering correction procedure that was made up of the sequence of K measures in the field, and data elaboration using the FV2200 software. On the same sampling areas, on suitable days (sky with homogeneous cloud cover), the samples were also carried out with the hemispherical photos and the subsequent processing using the open access code in R Hemiphot (Center and 2018, n.d.). The photographs were taken with a Nikon D3100 and a sigma 4.5mm f2.8, placing the camera at 1 m from the ground and with the top oriented to true North. The camera was set in manual mode with Iso 200, focal distance f. 8 and the minimum shutter speed was set to 1/30 s.